Critical issues in the heteroepitaxial growth of alkaline-earth oxides on silicon

J. Lettieri, J. H. Haeni, and D. G. Schlom

Articles you may be interested in

Theoretical investigation of the alkaline-earth dihydrides from relativistic all-electron, pseudopotential, and density-functional study
J. Chem. Phys. **126**, 104307 (2007); 10.1063/1.2437213

Interface formation during molecular beam epitaxial growth of neodymium oxide on silicon
J. Appl. Phys. **99**, 074105 (2006); 10.1063/1.2188051

Hetero-epitaxy of perovskite oxides on GaAs (001) by molecular beam epitaxy
Appl. Phys. Lett. **85**, 1217 (2004); 10.1063/1.1783016

In situ observation of epitaxial growth of [Au/Co/Cu] and [Cu/Co/Au] superlattices and their magnetic interface anisotropies
J. Appl. Phys. **90**, 5104 (2001); 10.1063/1.1413230

Stranski-Krastanov growth of Al on Cr layers during molecular-beam epitaxial growth and its influence on the structure of epitaxial (001) Al/Cr superlattices
J. Appl. Phys. **87**, 159 (2000); 10.1063/1.371838

Critical issues in the heteroepitaxial growth of alkaline-earth oxides on silicon

J. Lettieri, J. H. Haeni, and D. G. Schlom[a)]

Department of Materials Science and Engineering, The Pennsylvania State University, University Park, Pennsylvania 16803-6602

The critical aspects of the epitaxial growth of alkaline-earth oxides on silicon are described in detail. The step by step transition from the silicon to the alkaline-earth oxide as shown through reflection high energy electron diffraction is presented, with emphasis placed on the favorable interface stability, oxidation, structural, and strain considerations for each stage of the growth via molecular beam epitaxy. © *2002 American Vacuum Society.* [DOI: 10.1116/1.1482710]

I. INTRODUCTION

The union of dissimilar materials presents potentially the most significant challenge to heteroepitaxial growth. Unlike cases of homoepitaxy or growth of films that strongly resemble the character of their substrates (e.g., the heteroepitaxial growth of oxide films on oxide substrates or compound semiconductors on compound semiconductor substrates) growth of materials with very strongly differing chemical and structural natures often dictate new or more stringent growth concerns. The heteroepitaxial growth of oxides on silicon serves as a prime example.

Despite its inherent difficulty, the integration of epitaxial oxides with semiconductors, which has been widely investigated for years,[1–4] has virtually limitless potential. The heteroepitaxial growth of oxides on semiconductors, and specifically silicon, presents significant opportunities to harness the versatile superconducting, dielectric, magnetic, nonlinear optical, pyroelectric, piezoelectric, and ferroelectric properties of oxides, while simultaneously exploiting the properties of the underlying semiconductor. To create epitaxial structures in which the properties of the underlying silicon and overlying oxide film both attain their full potential, control of the silicon/oxide interface is critical. Growth on silicon, however, presents serious complications concerning reactivity between the desired oxide and silicon and delicate oxidation considerations. One demonstrated route that addresses the concerns of the transition from silicon to a more complex oxide (specifically perovskite) is through an intermediate alkaline-earth oxide.[5] In this article, we describe the crucial and advantageous aspects of the alkaline-earth oxide/silicon system, which enable these materials to grow in an epitaxial and highly crystalline manner. The step by step transition from the silicon to the alkaline-earth oxide as shown through reflection high energy electron diffraction (RHEED) is described in detail, with emphasis placed on the favorable interface stability, oxidation, structural, and strain considerations for each stage of the growth via molecular beam epitaxy (MBE). The purpose of this article is not to irrefutably resolve the many issues still open to debate in this field, but rather to explain critical ideas and demonstrate successful pathways to the growth of an alkaline-earth oxide on silicon.

II. EXPERIMENTAL PROCEDURE

The vacuum deposition chamber used to complete this work is shown schematically in Fig. 1. The chamber is an EPI 930 MBE[6] modified for the growth of oxides on silicon. The vacuum system contains two *in situ* diagnostic tools employed in these experiments: (1) RHEED to probe the film surface during growth and (2) a retractable quartz crystal microbalance (QCM) used to measure mass flux in the position of the wafer and conduct oxidation experiments. Fluxes were measured before and after deposition and showed less than 1% fluctuation over hours of growth. The system allows for independent control of nine elemental sources (including the oxidant sources) and employs computer control over furnaces, substrate heater, and shutters. The alkaline-earth metals used in this study (barium[7] and strontium[8]) were held in titanium crucibles and deposited onto a silicon substrate by thermal evaporation from low-temperature effusion cells. Gadolinium[9] was held in a tungsten crucible and deposited by thermal evaporation from a high-temperature effusion cell. The oxidant (99.9999% molecular O_2 plus 100 ppm N_2 for all growths) was introduced into the chamber through a needle valve connected to a tungsten tube with an outlet diameter of ≈ 0.6 cm a distance of ≈ 19 cm from the substrate. (This is an atomic hydrogen source.)[6] Background pressures were measured with an ion gauge located on the chamber wall ≈ 35 cm from the substrate. The pressures given are those indicated by the ion gauge and are uncorrected for the gas species being pure oxygen. The base pressure for the unbaked chamber was 2×10^{-9} Torr. Substrate temperatures above 500 °C were measured with an optical pyrometer[10] (assuming an emissivity of 0.8) aimed at the surface of the silicon substrate. Temperatures less than 500 °C were based on thermocouple measurements. The maximum deviation between thermocouple and pyrometer measurements occurred at high temperatures (e.g., at 1050 °C registered by the thermocouple, the pyrometer read 840 °C) with decreasing deviation down to room

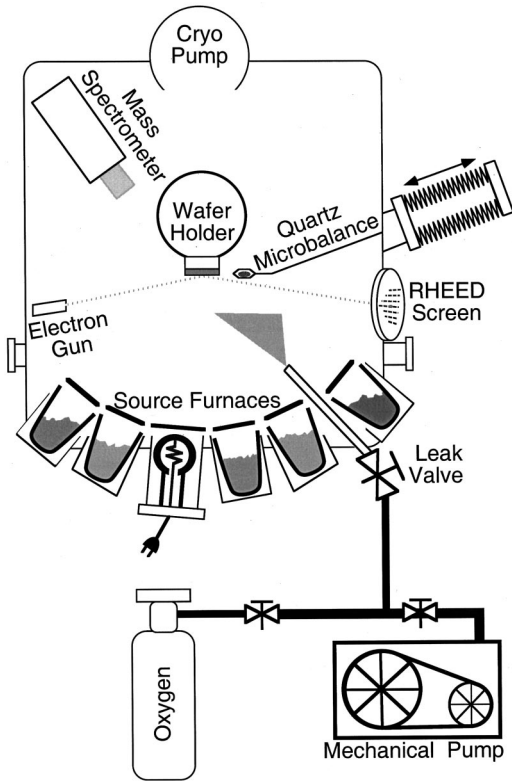[a)]Electronic mail: schlom@ems.psu.edu

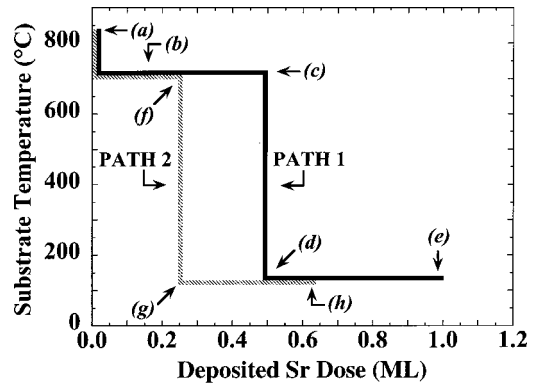FIG. 1. Schematic of the MBE growth chamber used for the deposition of alkaline-earth oxides on silicon.

FIG. 2. Process flow diagram showing the temperature and deposited strontium dose for two different growth paths. The diagram indicates that although the RHEED signature many vary slightly, some latitude exists in terms of strontium dosages that lead to epitaxial alkaline-earth oxide in subsequent steps. The letter labels correspond to the respective RHEED images in Fig. 3.

temperature. Details concerning the specific fluxes, substrate temperatures, and oxidant pressures are outlined in Sec. III.

Films were grown on 3 in. diam silicon[11] with (001) orientation held on molybdenum sample holders with pyrolytic boron nitride (pBN) retainer rings. All wafers used in this study were from the same boule and films were grown in succession to ensure consistency in the data.

III. RESULTS AND DISCUSSION

A. Thermodynamic stability criterion

Chemical reactivity plays a crucial role when examining heteroepitaxy in complex systems. To achieve high quality epitaxy, one needs to maintain a stable interface between the metal oxide and the silicon, and the loss of this interface through chemical reaction and the formation of interfacial phases (in this case silicates or amorphous silica and metal) will in a worst case, eliminate epitaxy. Although the consideration of chemical reactivity and thermodynamic stability is a critical concern for the growth of any thin film, this concern is magnified further when examining materials that are known to be extremely reactive (such as silicon) and in the most restrictive case of thin film growth, epitaxy.

Through consideration of thermodynamic stability along with other basic guidelines (i.e., solid and not radioactive), the choices for binary metal oxide on silicon epitaxy become severely restricted.[12] Indeed, the bulk of these materials fall into two classes of oxides, alkaline-earth oxides and rare-earth oxides. Given their demonstrated ability to grow in a

very low oxygen pressure and low temperature regime and previous success in their growth in a MBE environment,[5,13,14] alkaline-earth oxides are very promising candidates for oxide on silicon epitaxy.

B. Transition from silicon to alkaline-earth oxide–RHEED evolution

One of the easiest ways to describe the transition from silicon to alkaline-earth oxide is by examining the RHEED evolution through this process. Figure 2 shows various paths taken to effect the transition from silicon to alkaline-earth oxide. RHEED images along the [110] azimuth of silicon at different stages of the growth processes illustrated in Fig. 2 are shown in Fig. 3. These figures will be referred to extensively over the next few sections to describe the growth of the oxide. The variation in process temperature and alkaline-earth metal dose as outlined in Fig. 2 demonstrates that some latitude does exist in achieving an epitaxial alkaline-earth oxide on silicon. While some variation can be seen in the RHEED images in Fig. 3, the key elements (clean, reconstructed silicon surface, formation of a submonolayer silicide, and metal overlayer) are common to paths that will ultimately yield epitaxial oxides. These steps are described in detail in the next sections.

1. Reconstructed silicon

Since the goal of this work is achieving an abrupt crystalline interface, beginning the growth process with a clean, crystalline silicon surface is of critical importance. Excessive carbon contamination can lead to the formation of SiC, which will severely degrade the epitaxy in the layers that follow.[15] Figure 3(a) shows a RHEED image of a reconstructed, double-domain (2×1) Si surface, which represents the first step of this multistep growth. To obtain this surface, a silicon wafer was put under an ultraviolet (UV) lamp for 1 min (with the UV lamp creating a localized ozone atmosphere) as an ozone treatment and then loaded into the deposition chamber and heated in vacuum to 840 °C for 20 min.
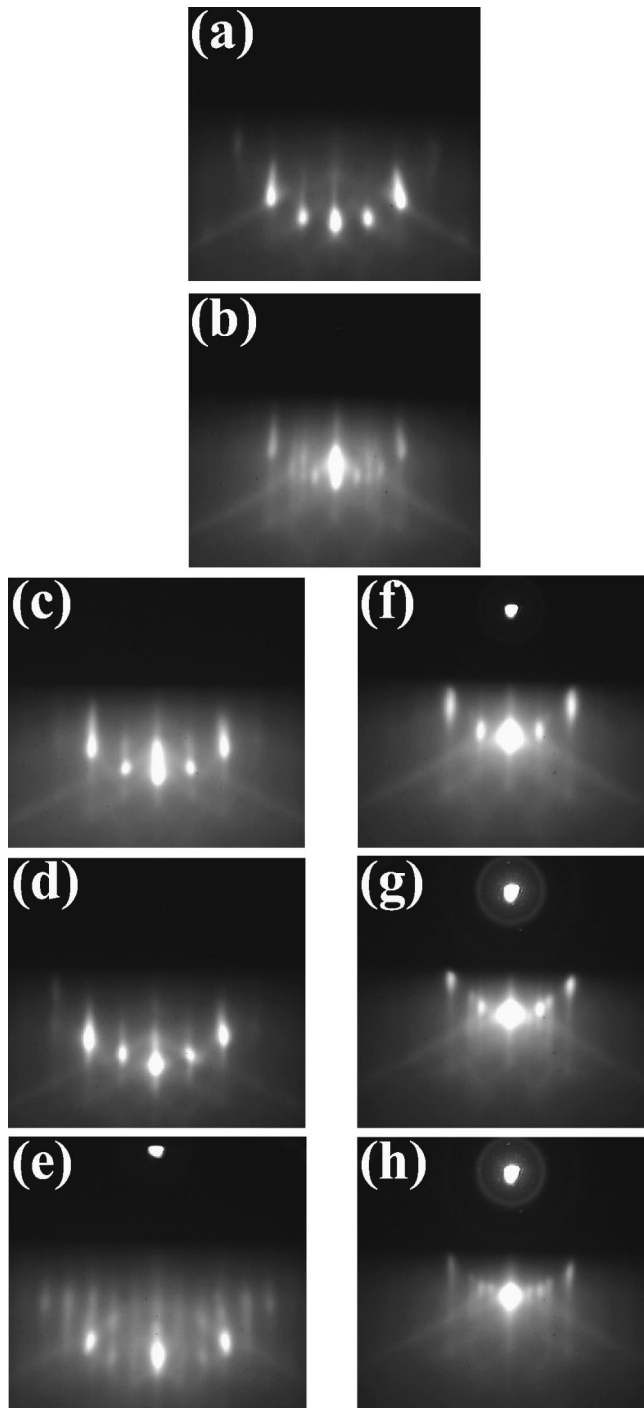
FIG. 3. RHEED images along the [110] azimuth of silicon taken at various stages of the growth for two distinct paths as outlined in Fig. 2. (a) (2×1) reconstructed silicon surface after heating in vacuum to temperatures above 840 °C for 20 min. (b) After the deposition of a 1/6 ML strontium dose at 700 °C, showing the evolution to a 3× pattern. PATH 1 (c) after the deposition of a 1/2 ML strontium dose at 700 °C, showing the return to the 2× pattern with a maximum intensity. (d) Same film shown in Fig. 3(c) after cooling to 120 °C. Note the *lack* of change in the pattern. (e) After the deposition of a 1/2 ML strontium dose deposited at 120 °C showing the formation of the 3× metal overlayer. PATH 2 (f) after the deposition of a 1/4 ML strontium dose at 700 °C. (g) Same film shown in Fig. 3(f) after cooling to 120 °C. Note the change from the previous pattern. (h) After the deposition of a 3/8 ML strontium dose deposited at 120 °C while following PATH 2. It should be noted that the RHEED images shown are all before the introduction of oxygen into the chamber. The flux of strontium for these two growths was 2×10^{13} atoms/cm^2 s.

All amorphous SiO_2 on the substrate surface, which could hinder epitaxy, must be eliminated prior to growth, and the (2×1) Si that results provides an excellent template for subsequent epitaxial growth.

2. Silicide formation

The second stage of the growth process is the deposition of the alkaline-earth metal (in this example strontium) and the formation of a submonolayer silicide at ~700 °C (see PATH 1 in Fig. 2). At a 1/6 monolayer (ML) of deposited strontium dose[16] the RHEED pattern evolves into a 3× reconstruction. At 1/2 ML of the deposited strontium dose, we see the RHEED return to a 2× pattern with maximum intensity [Figs. 3(b) and 3(c), respectively]. Although the true composition of the surface yielding the 1/2 order streaks remains an unresolved issue[5,17–19] and the determination of its exact nature remains a formidable task,[20,21] the character of the surface no longer resembles that of pure silicon, nor that of strontium metal.[19] In fact, the nomenclature itself of this layer remains a debatable issue. Previous work has predicted, that although a Sr–Si bond exists, the properties of such a layer do not resemble that of a bulk silicide, but rather that of a chemisorbed strontium on a silicon surface.[22] The semantics may or may not be a moot point, however, for ease of description in this article, this layer will be referred to as the ''submonolayer silicide.''

The formation of the submonolayer silicide is a critical step in the process, and we have achieved no success in situations where a silicide is not first grown. The complete role of this layer is multiple and complex. Principally, it forms an excellent template (in terms of lattice constant) for the subsequent growth of the oxide. Additionally, this silicide structure (based on RHEED observation) exhibits a much higher resistance to oxidation than the silicon surface alone, in agreement with Ref. 18. (The ultimate chemical nature of this interfacial silicide layer upon exposure to oxygen is discussed in Sec. III B 4.) Finally, the formation of the submonolayer silicide allows the next step of the transition, the deposition of an alkaline-earth metal overlayer.

As stated previously, there is a dosage window in terms of deposited strontium that leads to epitaxial oxide growth. This can be seen by following the dotted path (PATH 2) on Fig. 2 where instead of 1/2 ML, a 1/4 ML silicide is grown. Although the RHEED evolution is slightly different, the deposition of the 1/4 ML presents a viable path to epitaxial growth [Figs. 3(f), 3(g), and 3(h)].

3. Alkaline-earth–metal deposition

For the next step of the transition, (see Fig. 2) the substrate temperature is cooled considerably and additional alkaline-earth metal is deposited until the RHEED pattern in Fig. 3(e) is observed, which is indicative of an ordered 3× structure. Slight changes in substrate temperature will have a significant effect on the quality of this ordered strontium metal overlayer, which can be observed even when deposited at room temperature. The pattern in Fig. 3(e) shows a RHEED image resulting from the deposition at 120 °C. The

quality of this $3\times$ reconstruction will not limit one's ability to grow epitaxial alkaline-earth oxide in the next step. The critical idea, however, is that this heteroepitaxial stack now consists of the silicon substrate, submonolayer silicide, and submonolayer metal overlayer. In many other systems (including several rare earths) similar behavior is not observed.[23] Often the further deposition of metal will result in the formation of a thick silicide layer even at room temperature.[24] Formation of a thick silicide in many cases can lead to decreased crystalline quality and multiple film orientations. Additionally, in many applications (i.e., where a field effect between the overlying dielectric or ferroelectric and underlying silicon is desired) the formation of a thick silicide should be avoided to prevent the screening of the desired field effect by this intermediate silicide layer. The formation of a stable submonolayer silicide and subsequent metal overlayer, which is a relatively uncommon phenomenon, makes alkaline-earth metals and oxides so amenable to this process. This metal overlayer, which plays a role in the initial stages of oxidation, will be explained in more detail in the next section.

As with the previous layer, the true nature of the layer in this third step of the deposition is not definitively clear. Conclusive determination of the character of this layer as a metal is ambiguous at best, even through the use of high-resolution x-ray photoelectron spectroscopy.[18] However, based on previous low energy electron diffraction studies[25] and our own work looking at oxidation of this layer, it is consistent with a physisorbed metallic strontium overlayer or (again, for ease of description) a "submonolayer metal." Furthermore, epitaxial alkaline-earth oxide can be obtained over a range of strontium dosage at this stage. An epitaxial oxide has been grown for deposited strontium doses ranging from 3/8 to 1 ML (although the $3\times$ reconstruction will disappear), which gives credence to the idea that this layer is, in fact, a metal which incorporates into the film during the onset of oxidation in the next step of the process. (Potentially an even thicker strontium metal layer could be successful, however, we have explored only up to 1 ML of deposited strontium dose.)

4. Oxidation

Perhaps the most important step in the entire transition from silicon to alkaline-earth oxide is the introduction of the oxidant into the system. Since the formation of SiO_2 (especially at the earliest stages of the growth) can have a strongly limiting effect on the quality of the subsequent epitaxial oxide growth, one would like to minimize the overall oxygen pressure in the system. Historically, three strategies have been used to grow epitaxial oxides on silicon. The ultimate goal of all three methods is to avoid the formation of an amorphous SiO_2 layer that would result in the loss of the substrate's crystalline template before the oxide has a chance to nucleate on it. The first strategy is to grow it with no excess oxidant.[26–29] This could be achieved, for example, through the use of a single reactant species having a stoichiometric composition, e.g., by the supply of BaO molecules to the substrate surface. As most oxides do not evaporate congruently, the supply of stoichiometric molecules of the desired oxide to the substrate is a rare case unless nonequilibrium evaporation techniques or specialized chemical precursors are used. Nonetheless, it has been used recently to grow Y_2O_3,[26,27] CeO_2,[28] Pr_2O_3,[29] and Gd_2O_3[26,27] epitaxial films on silicon. An easier way to deposit films is to use an excess oxidant environment, and the remaining two methods involve oxidant-rich growth conditions. The excess oxidant flux helps ensure that the grown film will be fully oxidized. To prevent oxidation of the silicon substrate during the critical nucleation stage, two regimes of substrate temperature have been demonstrated for excess oxygen growth conditions: (1) high temperature, where SiO has sufficient volatility to keep the silicon surface free of SiO_2 for a low flux of oxidant and (2) low temperature, where the oxidation of silicon by the oxidant is sluggish due to kinetics. Most reports of the epitaxial growth of oxides on silicon fall into the high temperature/excess oxygen regime.[3,30–65] Although successful for the nucleation of an epitaxial oxide layer, these growth conditions typically lead to the growth of a SiO_2 layer at the silicon interface as the film thickens (and SiO can no longer make its way to the film surface to evaporate) due to the oxygen-rich growth conditions and high diffusivity of oxygen at the high growth temperature. When a SiO_2-free interface is required, either the first or the last of these three methods is desired. As the first can rarely be satisfied, the last of the three methods, the low temperature/excess oxygen regime, is appealing.[5,37,66] Indeed, alkaline-earth oxides can be grown epitaxially on silicon with great control in this third regime. They can also be grown in the high temperature/excess oxidant regime, but with the concomitant danger of SiO_2 formation.[31–38,64,65] It is in this low temperature/excess oxidant regime that assessing kinetic barriers to oxidation of the species being supplied to the substrate is critical. As a result, the threshold for oxidation of the alkaline-earth metal, i.e., the absolute minimum pressure where one can oxidize the metal and grow a film, represents an important process parameter.

Establishment of this oxidation threshold is determined through a separate *in situ* experiment where alkaline-earth metal is deposited in the presence of O_2 onto a QCM. Mass accumulation rate is measured as a function of O_2 partial pressure. Similar techniques have been used previously to look at oxidation of other metal systems.[67,68] Data from this type of experiment for the oxidation of strontium, barium, and gadolinium are shown in Figs. 4(a), 4(b), and 4(c), respectively. These plots show mass accumulation rate and O_2 partial pressure as a function of time. The labeled, solid dark lines indicate the position corresponding to the mass accumulation rate of the pure metal and fully oxidized alkaline-earth metal oxide (or rare-earth metal oxide in the case of the gadolinium).

Based on the data collected and plotted in Fig. 4 the plot in Fig. 5 was generated. One can see the onset of oxidation of strontium at pressures less than 3×10^{-9} Torr and complete oxidation of the strontium at pressures in the range of 8×10^{-8} Torr for this deposition flux
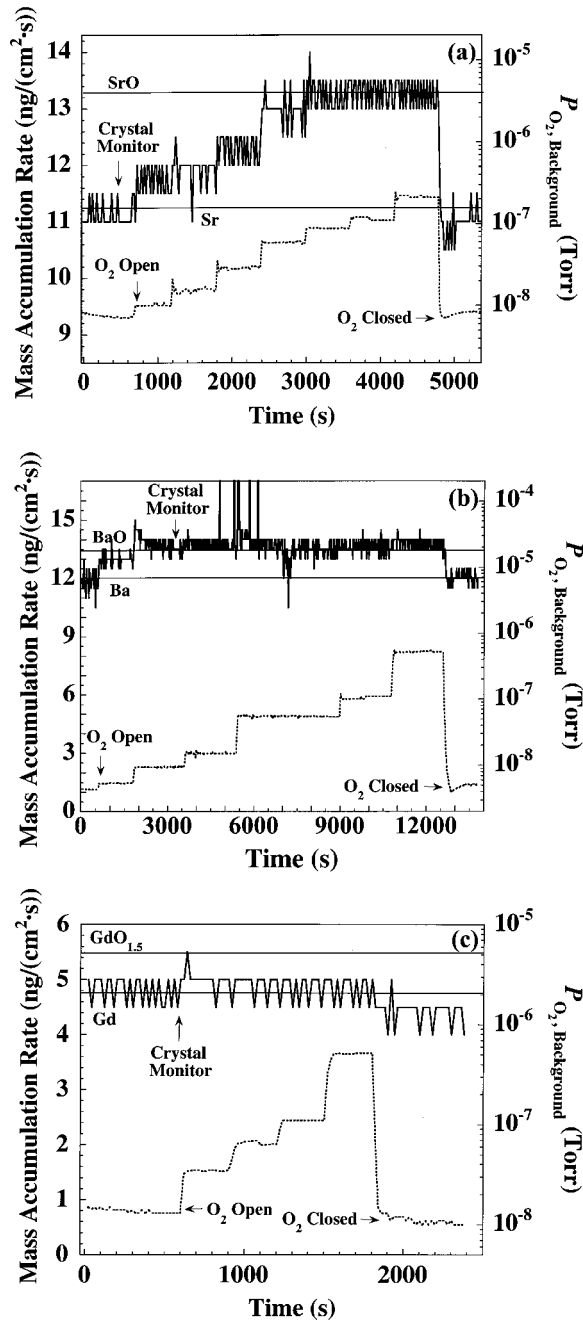
FIG. 4. Graphs showing mass accumulation rate on the QCM as a function of time for varying O_2 partial pressures for (a) strontium, (b) barium, and (c) gadolinium. The labeled, horizontal lines indicate the positions corresponding to the deposition of the pure metal and fully oxidized metals. From the plots one can see the general ease of oxidation of the strontium and barium in contrast with the general difficulty in oxidizing the gadolinium. All experiments were conducted at room temperature with a metallic flux of $(2-7) \times 10^{13}$ atoms/cm^2 s.

($\sim 7 \times 10^{13}$ Sr atoms/cm^2 s). The oxidation of barium shown in Fig. 4(b) occurs at even lower pressures with the complete oxidation of the barium metal at pressures in the low 10^{-9} Torr range. For comparison and contrast, the analogous oxidation data for gadolinium [Fig. 4(c)] shows that at oxygen pressures in excess of 7×10^{-7} Torr, we do not even see the onset of oxidation in this rare-earth metal.
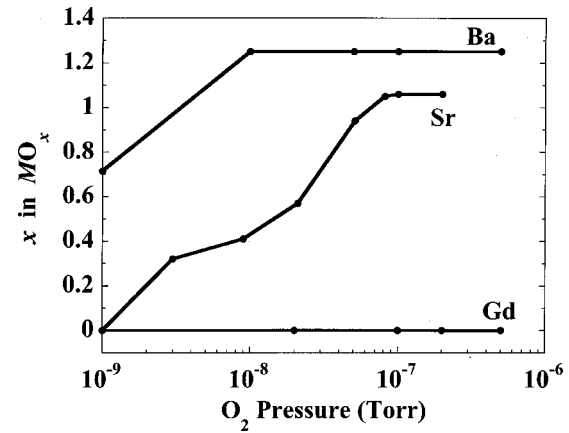

FIG. 5. Plot showing degree of oxidation for strontium, barium, and gadolinium metal as a function of O_2 partial pressure. This plot was generated directly from the data shown in Fig. 4.

The ramifications of this study are fortuitous. The general ease of oxidation (at low temperatures) of the alkaline-earth metals make them especially well suited to growth on silicon, where unwanted oxidation of the substrate is a critical concern. (The bare silicon substrate, for example, will form 0.5 ML of oxide at room temperature upon exposure to 1×10^{-6} Torr O_2 for less than 10 s).[69]

The general growth procedure that has yielded consistently high quality results has been to slowly increase the partial pressure of oxygen into the chamber to a background pressure of approximately 5×10^{-9} Torr and then begin depositing the alkaline-earth metal, while simultaneously raising the oxygen pressure to approximately 3×10^{-8} Torr. One of the functions of the deposited metal overlayer described in the previous section is to help ease the transition into the formation of the oxide. This can be seen through inspection of the RHEED as the $3\times$ metal overlayer evolves to a $1\times$ metal over layer, while the oxygen partial pressure is increased to 5×10^{-9} Torr. A continued increase of the oxygen pressure in this step or beginning the deposition of the alkaline-earth metal too slowly will result in diminished epitaxial quality and some amorphous content, which can be
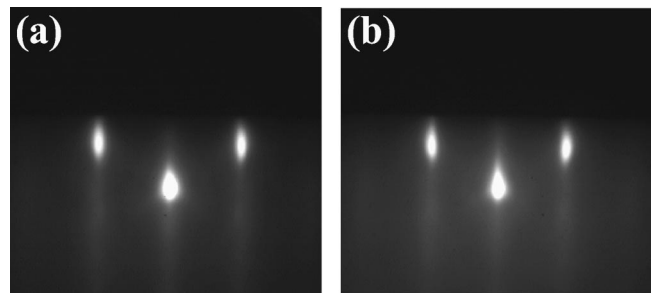

FIG. 6. (a) RHEED image along the [110] azimuth of silicon after the growth of 3 ML of Ba$_{0.70}$Sr$_{0.30}$O grown following PATH 1 as shown in Fig. 2. (b) RHEED image along the [110] azimuth of silicon after the growth of 3 ML of Ba$_{0.70}$Sr$_{0.30}$O grown following PATH 2 as shown in Fig. 2. The epitaxial relationship is described as (001) Ba$_{0.70}$Sr$_{0.30}$O ∥ (001) Si and [100] Ba$_{0.70}$Sr$_{0.30}$O ∥ [100] Si. These two images demonstrate the ability to grow epitaxial alkaline-earth oxides using various deposition paths.

seen in the RHEED. When the procedure is implemented in the correct pressure regime the patterns in Figs. 6(a) and 6(b) result.

The patterns shown in Fig. 6 are from the growth of lattice matched (Ba, Sr)O on (001) silicon (lattice matching and solid solution of the alkaline-earth oxides are addressed in the next section). Seemingly, the growth pressure outlined above (3×10^{-8} Torr) is below the pressure required for the full oxidation of the strontium metal (see Fig. 5). Due to the catalytic oxidation behavior of the codeposited barium, however, the strontium being codeposited with barium becomes oxidized to SrO at lower pressures than needed for the oxidation of strontium when it is deposited alone. Similar behavior has been reported in the oxidation of other elements, e.g., silicon and aluminum, though the use of an alkali metal catalyst and has been attributed to surmounting kinetic barriers to oxidation.[70–72] We have seen similar behavior with the alkaline earth metals. In their previous work on alkali metals,[70] Braaten et al. attribute this type of catalytic behavior to the ability of an easily oxidized metal to increase the rate of dissociation of oxygen at the substrate surface. These results support the trend that lower work function materials result in higher oxygen incorporation.[70] Analogous results are demonstrated here with the alkaline earths.[68]

Questions still exist concerning the ultimate composition and structure of the interfacial silicide upon exposure of the silicon/silicide/metal stack to oxygen. Based on first principles calculations, Droopad et al. have predicted the transformation of the silicide layer to a silicate in the presence of oxygen.[17] Silicate formation has been observed under related growth conditions.[18] The stability of this layer in an oxygen environment might suggest a transformation to a silicate. Whereas an alkaline-earth metal/silicon interface might lead to promoted oxidation of the underlying silicon[73,74] (through the catalytic behavior described above), the formation of a silicate could serve as a protective layer and stem the formation of amorphous SiO_2. As with the silicide, questions of nomenclature exist, and the most correct terminology for the interface may be described as "a layer consisting of silicon, strontium, and oxygen," however the true chemistry is still debated.

C. Low-temperature growth and lattice matching

Besides the advantageous oxidation behavior described in the previous section, alkaline-earth oxides are able to grow epitaxially at extremely low temperatures due to the highly ionic nature of their bonding.[75] For example, epitaxial growth of MgO has previously been demonstrated at temperatures down to 140 K.[13] The patterns shown in Fig. 6 were taken for films grown at room temperature. Reduction of the growth temperature not only minimizes the potential for diffusion and interface reaction, but also minimizes the possibility of unwanted oxidation of the silicon substrate. From a process control and repeatability perspective, this third regime for the growth of epitaxial oxides on silicon (see Sec. III B 4) is the best. The extremely low temperatures at which the alkaline-earth oxide layer may be grown epitaxi-
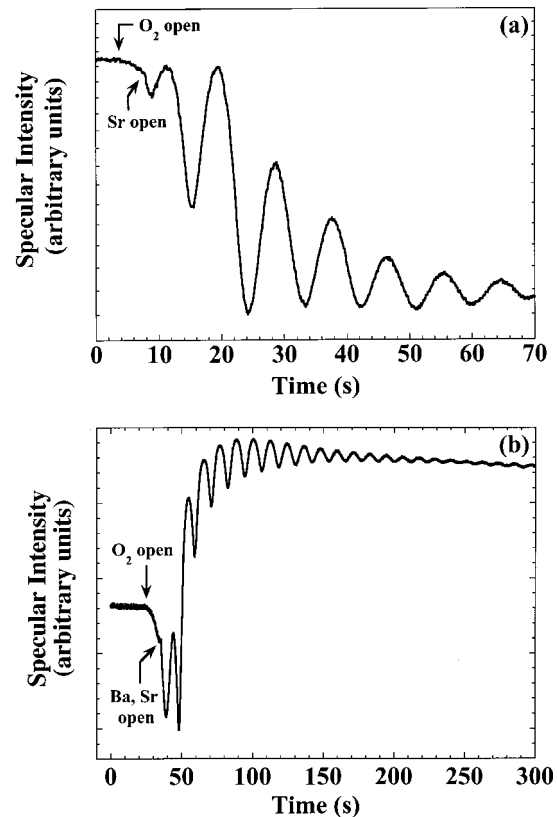
FIG. 7. RHEED intensity oscillations of the specularly reflected spot along the [110] azimuth of silicon at 25 °C during deposition in 3×10^{-8} Torr O_2 for: (a) SrO and (b) lattice-matched (Ba, Sr)O. The oscillations of the mismatched SrO show a decreasing intensity and dampening of oscillations.

ally makes this desired regime accessible for the growth of lattice-matched (Ba, Sr)O epitaxial layers on silicon.

Another critical advantage to the alkaline-earth oxides is the ability to tune the lattice constant over a wide range of values utilizing solid solutions of different alkaline-earth oxide constituents. Given the lattice constant of silicon, 5.43 Å, the solid solution of $Ba_{0.72}Sr_{0.28}O$ results in a perfectly lattice-matched oxide. Despite the significant miscibility gap known to exist in the BaO–SrO system,[76] work by Hellman and Hartford previously demonstrated complete solid solution for SrO–CaO thin films (another alkaline-earth oxide system with a complete miscibility gap in bulk form) grown on MgO at room temperature.[14] Enhanced miscibility in epitaxial films versus bulk is well established in other systems,[77,78] including oxides.[79] Here similar results are seen (complete solid solution) for the growth of $Ba_xSr_{1-x}O$ on silicon. This solid solubility allows for the tuning of the lattice constant of the oxide to be either perfectly latticed matched to the silicon to create a coherent interface, or optionally modified to engineer an intentional strain, which has been shown to modify the properties of strained epitaxial layers in other systems.[80,81] The implications and differences between growing a lattice-matched oxide and a nonlattice-matched oxide can be seen clearly in the RHEED intensity oscillations during growth. Figures 7(a) and 7(b) show RHEED intensity oscillations of the specularly reflected spot
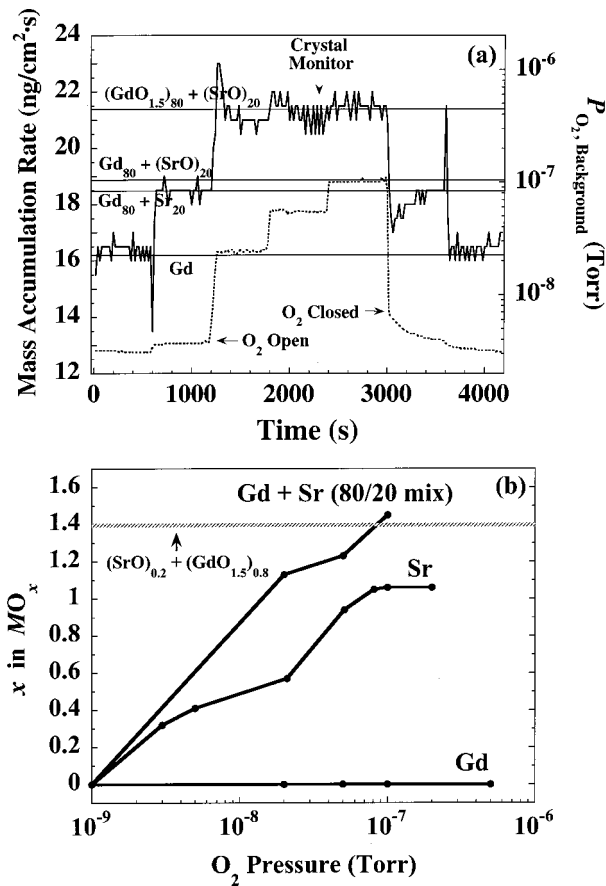
FIG. 8. (a) Graph similar to the plots shown in Fig. 4 showing mass accumulation rate on the QCM as a function of time for varying O_2 partial pressures for a 80% Gd/20% Sr mix. (b) Plot showing degree of oxidation for strontium, gadolinium, and a 80% Gd/20% Sr mix as a function of O_2 partial pressure. The plot demonstrates the catalytic nature of the alkaline earth and indicates that full oxidation occurs orders of magnitude lower than for the deposition of the pure gadolinium metal alone.
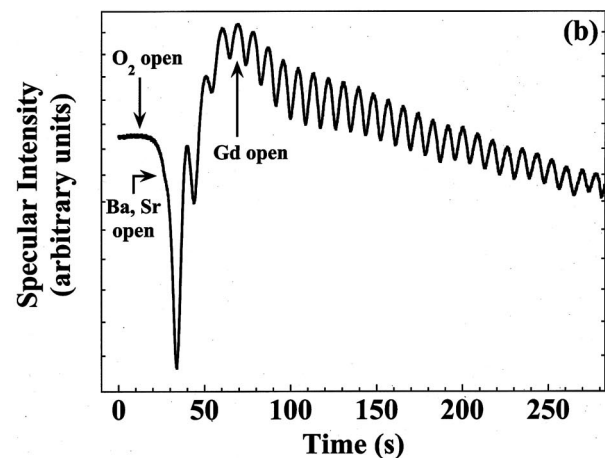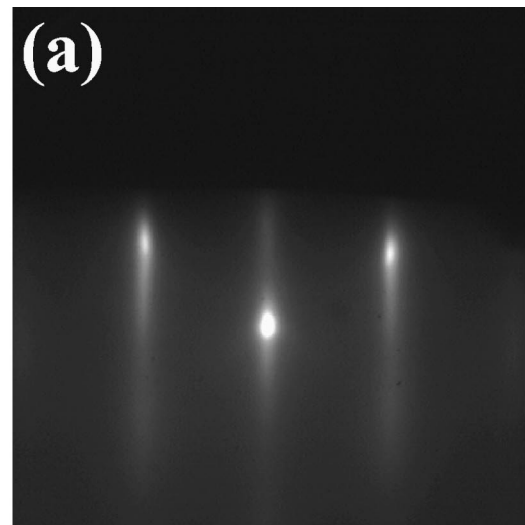
FIG. 9. (a) RHEED image along the [110] azimuth of silicon after the growth of 25 ML of 16% Gd-doped $Ba_{0.70}Sr_{0.30}O$ ($Ba_{0.59}Sr_{0.25}Gd_{0.16}O_y$) grown at 25 °C and 3×10^{-8} Torr and (b) corresponding RHEED intensity oscillations from the specularly reflected reflection.

(along the [110] azimuth of silicon) for pure SrO and lattice-matched (Ba, Sr)O, respectively, grown on (001) silicon at 25 °C. The oscillations for the mismatched SrO show markedly decreasing intensity and dampening of the oscillations, in direct contrast to the oscillations shown in Fig. 7(b). The sharp decrease is due to relaxation of the mismatched SrO at a very small critical thickness; analogous RHEED oscillations have been reported for mismatched compound semiconductor heteroepitaxy.[82]

D. Rare-earth doped alkaline-earth oxides

Alkaline-earth oxides show significant promise for silicon integration, however they are still plagued by some major limitations. For example, although stable in direct contact with silicon at low temperatures, BaO will react with silicon at elevated temperatures.[83–85] Such reaction is consistent with thermodynamic predictions.[12] If a film (such as the one represented in Fig. 6) is heated to temperature above 630 °C (as measured by an optical pyrometer) the pattern will become amorphous (as seen by RHEED).[83,86] Reaction with the carbon dioxide and water vapor in air also proves to be a

serious limitation for many of the alkaline-earth oxides. One potential solution to improve these properties is to grow solid solutions of alkaline earth and rare-earth oxides (e.g., Gd_2O_3 as demonstrated here), since rare-earth oxides show significantly improved stability in air as well as temperature stability when in contact with silicon.

Although oxidation of a pure rare earth such as gadolinium with the oxidant used in this study [see Fig. 4(c)] is not possible in the low pressure regimes utilized in this process, the deposition of gadolinium in the presence of the alkaline-earth constituent (which plays the dual role as an oxidation catalyst)[68] makes full oxidation and subsequent growth possible. The plot in Fig. 8(a) shows the QCM oxidation data for an 80% Gd/20% Sr mix. Figure 8(b) (similar to the plot generated in Fig. 5) shows the oxidation behavior for the strontium, gadolinium, and gadolinium/strontium mixture. The data indicate that oxidation of the gadolinium in the presence of an alkaline earth occurs at pressures orders of magnitude below those required to oxidize pure gadolinium. It is important to note when looking at this graph,

that although the oxidation line for the gadolinium/strontium mixture lies to the left of the pure strontium metal line, full oxidation occurs at lower pressures for the pure strontium deposition. This is due to the fact that the x for a fully oxidized SrO_x is 1.0 while for a fully oxidized $Gd_{0.8}Sr_{0.2}O_x$ mixture $x = 1.4$.

As with the alkaline earths, there exists very little solid solubility between alkaline earth and rare-earth oxides at low temperatures. The phase diagram for $BaO-Gd_2O_3$ has not been determined, however, other alkaline-earth oxide–rare-earth oxide systems show little or no solid solubility even at elevated temperatures.[87–91] Like the previous case, the bulk phase diagram does not correspond to what is seen in thin film form (i.e., very large regions of solid solubility). Figure 9 shows a RHEED image at the completion of growth along the [110] azimuth of silicon and corresponding RHEED oscillations from the specular reflection for 25 ML of 16% Gd-doped $Ba_{0.70}Sr_{0.30}O$, i.e., $Ba_{0.59}Sr_{0.25}Gd_{0.16}O_y$ demonstrating the ability to grow these solid solutions. The frequency of the RHEED oscillations as well as the absence of impurity phases in the RHEED patterns are fully consistent with the 16% Gd in this film going into the rock salt structure of (Ba, Sr)O. Despite the significant rare-earth oxide content, reaction between the film and underlying silicon was observed and an amorphous reaction product still formed at $\sim 600\,°C$.

IV. CONCLUSIONS

The successful growth of epitaxial alkaline-earth oxides on silicon requires an understanding of the interface on a submonolayer level. One demonstrated transition from semiconductor to oxide has been described in detail in this article by examination of this pathway through *in situ* RHEED. The steps outlined above represent the crucial aspects of these growths and provide insight into the potential growth of other oxides on silicon.

ACKNOWLEDGMENTS

[1] T. Yamaguti, Proc. Phys. Math. Soc. Jpn. **17**, 443 (1935).

[2] R. Sato, J. Phys. Soc. Jpn. **6**, 527 (1951).

[3] M. Ihara, Y. Arimoto, M. Jifuku, T. Kimura, S. Kodama, H. Yamawaki, and T. Yamaoka, J. Electrochem. Soc. **129**, 2569 (1982).

[4] S. Matsubara, N. Shohata, and M. Mikami, Jpn. J. Appl. Phys., Suppl. **24**, 10 (1985).

[5] R. A. McKee, F. J. Walker, and M. Chisholm, Phys. Rev. Lett. **81**, 3014 (1998).

[6] Applied EPI, St. Paul, MN.

[7] Aldrich-APL, Urbana, IL, 99.99% pure.

[8] Aldrich-APL, Urbana, IL, 99.99% pure.

[9] Alfa Aesar, 99.9% pure.

[10] Minolta/Land Cyclops 152, Osaka, Japan.

[11] Virginia Semiconductor, Inc. Fredericksburg VA (single side polished, (001) ± 0.1°, phosphorous doped, 1.0–10.0 $\Omega\cdot$cm resistivity).

[12] K. J. Hubbard and D. G. Schlom, J. Mater. Res. **11**, 2757 (1996).

[13] S. Yadavalli, M. H. Yang, and C. P. Flynn, Phys. Rev. B **41**, 7961 (1990).

[14] E. S. Hellman and E. H. Hartford, Jr., Appl. Phys. Lett. **64**, 1341 (1994).

[15] F. J. Walker and R. A. McKee (unpublished).

[16] 1 ML is defined as the concentration of atoms on the (001) surface of silicon, i.e., 6.78×10^{14} atoms/cm^2.

[17] R. Droopad *et al.*, J. Cryst. Growth **227–228**, 936 (2001).

[18] Y. Liang, S. Gan, and M. Engelhard, Appl. Phys. Lett. **79**, 3591 (2001).

[19] A. Herrera-Gomez, F.S. Aguirre-Tostado, Y. Sun, P. Pianetta, Z. Yu, D. Marshall, R. Droopad, and W. E. Spicer, J. Appl. Phys. **90**, 6070 (2001).

[20] X-ray photoelectron spectroscopy (XPS) would potentially provide the most useful data to answer this question. Given the fact that the "silicide" layer is submonolayer and provides a minimal signal compared to the silicon substrate and the near overlap of the $2p$ binding energy that exists in the peaks in an XPS spectrum for silicon (~ 98.8–99.5 eV) and a silicide (~ 99.5–99.8 eV), conclusive determination remains elusive.

[21] J. F. Moulder, W. F. Stickle, P. E. Sobol, and K. E. Bomben, *Handbook of X-ray Photoelectron Spectroscopy* (Perkin Elmer Corp., Eden Prairie, MN, 1992).

[22] J. Wang (personal communication).

[23] V. G. Lifshits, A. A. Saranin, and A. V. Zotov, *Surface Phases on Silicon: Preparation, Structures, and Properties*, 1st ed. (Wiley, New York, 1994).

[24] W. A. Henle, M. G. Ramsey, F. P. Netzer, and S. Witzel, Surf. Sci. **243**, 141 (1991).

[25] W. C. Fan, N. J. Wu, and A. Ignatiev, Phys. Rev. B **42**, 1254 (1990).

[26] J. Kwo *et al.*, Appl. Phys. Lett. **77**, 130 (2000).

[27] J. Kwo *et al.*, J. Appl. Phys. **89**, 3920 (2001).

[28] J. T. Jones, E. T. Croke, C. M. Garland, O. J. Marsh, and T. C. McGill, J. Vac. Sci. Technol. B **16**, 2686 (1998).

[29] J. P. Liu, P. Zaumseil, E. Bugiel, and H. J. Osten, Appl. Phys. Lett. **79**, 671 (2001).

[30] D. K. Fork, F. A. Ponce, J. C. Tramontana, and T. H. Geballe, Appl. Phys. Lett. **58**, 2294 (1991).

[31] Y. Kado and Y. Arita, J. Appl. Phys. **61**, 2398 (1987).

[32] Y. Kado and Y. Arita, Extended Abstracts of the 18th (1986) International Conference on Solid State Devices and Materials, Tokyo, Japan, 1986, p. 45.

[33] H. Mori and H. Ishiwara, Jpn. J. Appl. Phys., Part 2 **30**, L1415 (1991).

[34] H. Ishiwara, H. Mori, K. Jyokyo, and S. Ueno, Mater. Res. Soc. Symp. Proc. **220**, 595 (1991).

[35] O. Nakagawara, M. Kobayashi, Y. Yoshino, Y. Katayama, H. Tabata, and T. Kawai, J. Appl. Phys. **78**, 7226 (1995).

[36] T. Tambo, K. Maeda, A. Shimizu, and C. Tatsuyama, J. Appl. Phys. **86**, 3213 (1999).

[37] R. A. McKee, F. J. Walker, J. R. Conner, E. D. Specht, and D. E. Zelmon, Appl. Phys. Lett. **59**, 782 (1991).

[38] Y. Kado and Y. Arita, Extended Abstracts of the 20th (1988 International) Conference on Solid State Devices and Materials, Tokyo, Japan, 1988, p. 181.

[39] H. Fukumoto, T. Imura, and Y. Osaka, Appl. Phys. Lett. **55**, 360 (1989).

[40] H. Fukumoto, M. Yamamoto, and Y. Osaka, Proc.-Electrochem. Soc. **90**, 239 (1990).

[41] K. Harada, H. Nakanishi, H. Itozaki, and S. Yazu, Jpn. J. Appl. Phys., Part 1 **30**, 934 (1991).

[42] S. C. Choi, M. H. Cho, S. W. Whangbo, C. N. Whang, S. B. Kang, S. I. Lee, and M. Y. Lee, Appl. Phys. Lett. **71**, 903 (1997).

[43] M.-H. Cho, D.-H. Ko, Y. K. Choi, I. W. Lyo, K. Jeong, T. G. Kim, J. H. Song, and C. N. Whang, J. Appl. Phys. **89**, 1647 (2001).

[44] E. J. Tarsa, J. S. Speck, and McD. Robinson, Appl. Phys. Lett. **63**, 539 (1993).

[45] H. Nagata, M. Yoshimoto, T. Tsukahara, S. Gonda, and H. Koinuma, Mater. Res. Soc. Symp. Proc. **202**, 445 (1991).

[46] M. Morita, H. Fukumoto, T. Imura, Y. Osaka, and M. Ichihara, J. Appl. Phys. **58**, 2407 (1985).

[47] Y. Osaka, T. Imura, Y. Nishibayashi, and F. Nishiyama, J. Appl. Phys. **63**, 581 (1988).

[48] H. Myoren, Y. Nishiyama, H. Fukumoto, H. Nasu, and Y. Osaka, Jpn. J. Appl. Phys., Part 1 **28**, 351 (1989).

[49] P. Legagneux, G. Garry, D. Dieumegard, C. Schwebel, C. Pellet, G. Gautherin, and J. Siejka, Appl. Phys. Lett. **53**, 1506 (1988).

[50]H. Fukumoto, T. Imura, and Y. Osaka, Jpn. J. Appl. Phys., Part 2 **27**, L1404 (1988).

[51]H. Fukumoto, M. Yamamoto, Y. Osaka, and F. Nishiyama, J. Appl. Phys. **67**, 2447 (1990).

[52]H. Fukumoto, M. Yamamoto, and Y. Osaka, J. Appl. Phys. **69**, 8130 (1991).

[53]D. K. Fork, D. B. Fenner, G. A. N. Connell, J. M. Phillips, and T. H. Geballe, Appl. Phys. Lett. **57**, 1137 (1990).

[54]D. K. Fork, D. B. Fenner, R. W. Barton, J. M. Phillips, G. A. N. Connell, J. B. Boyce, and T. H. Geballe, Appl. Phys. Lett. **57**, 1161 (1990).

[55]D. K. Fork, F. A. Ponce, J. C. Tramontana, N. Newman, J. M. Phillips, and T. H. Geballe, Appl. Phys. Lett. **58**, 2432 (1991).

[56]D. B. Fenner, A. M. Viano, D. K. Fork, G. A. N. Connell, J. B. Boyce, F. A. Ponce, and J. C. Tramontana, J. Appl. Phys. **69**, 2176 (1991).

[57]W. Prusseit, S. Corsépius, M. Zwerger, P. Berberich, H. Kinder, O. Eibl, C. Jaekel, U. Breuer, and H. Kurz, Physica C **201**, 249 (1992).

[58]M. Ishida, I. Katakabe, T. Nakamura, and N. Ohtake, Appl. Phys. Lett. **52**, 1326 (1988).

[59]K. Sawada, M. Ishida, T. Nakamura, and N. Ohtake, Appl. Phys. Lett. **52**, 1672 (1988).

[60]H. Iizuka, K. Yokoo, and S. Ono, Appl. Phys. Lett. **61**, 2978 (1992).

[61]H. Wado, T. Shimizu, and M. Ishida, Appl. Phys. Lett. **67**, 2200 (1995).

[62]M. Ihara, Microelectron. Eng. **1**, 161 (1983).

[63]M. Mikami, Y. Hokari, K. Egami, H. Tsuya, and M. Kanamori, *Extended Abstracts of the 15th Conference on Solid State Devices and Materials* (Japan Society Applied Physics, Tokyo, 1983), pp. 31–34.

[64]K. Eisenbeiser *et al.*, Appl. Phys. Lett. **76**, 1324 (2000).

[65]Z. Yu, J. Ramdani, J. A. Curless, C. D. Overgaard, J. M. Finder, R. Droopad, K. W. Eisenbeiser, J. A. Hallmark, W. J. Ooms, and V. S. Kaushik, J. Vac. Sci. Technol. B **18**, 2139 (2000).

[66]M. Yoshimoto, K. Shimozono, T. Maeda, T. Ohnishi, M. Kumagai, T. Chikyow, O. Ishiyama, M. Shinohara, and H. Koinuma, Jpn. J. Appl. Phys., Part 2 **34**, L688 (1995).

[67]C. D. Theis and D. G. Schlom, in *High Temperature Materials Chemistry IX*, edited by Karl Spear (Electrochemical Society, Pennington, NJ, 1997), Vol. 97–39, pp. 610–616.

[68]J. Lettieri, J. Rodriguez Contreras, V. Vaithyanathan, and D. G. Schlom (unpublished).

[69]E. G. Keim, L. Wolterbeek, and A. Van Silfhout, Surf. Sci. **180**, 565 (1987).

[70]N. A. Braaten, J. K. Grepstad, S. Raaen, and S. L. Qui, Surf. Sci. **250**, 51 (1991).

[71]P. Soukiassian, T. M. Gentle, M. H. Bakshi, and Z. Hurych, J. Appl. Phys. **60**, 4339 (1986).

[72]Y. Huttel, E. Bourdie, P. Soukkiassian, P. S. Mangat, and Z. Hurych, Appl. Phys. Lett. **62**, 2437 (1993).

[73]A. Mesarwi, W. C. Fan, and A. Ignatiev, J. Appl. Phys. **68**, 3609 (1990).

[74]W. C. Fan and A. Ignatiev, Phys. Rev. B **44**, 3110 (1991).

[75]M. H. Yang and C. P. Flynn, Phys. Rev. Lett. **62**, 2476 (1989).

[76]K. T. Jacob and V. Varghese, J. Mater. Chem. **5**, 1059 (1995).

[77]T. Waho, S. Ogawa, and S. Maruyama, Jpn. J. Appl. Phys. **16**, 1875 (1977).

[78]A. Fischer, Z. Feng, E. Bykov, G. Contreras-Puente, A. Compaan, F. de Landa Castillo-Alvarado, J. Avendano, and A. Mason, Appl. Phys. Lett. **70**, 3239 (1997).

[79]H. Holzschuh and H. Suhr, Appl. Phys. Lett. **59**, 470 (1991).

[80]H. Schlotterer, Solid-State Electron. **11**, 947 (1968).

[81]A. C. Ipri and J. N. Zemel, J. Appl. Phys. **44**, 744 (1973).

[82]P. R. Berger, K. Chang, P. Bhattacharya, J. Singh, and K. K. Bajaj, Appl. Phys. Lett. **53**, 684 (1988).

[83]J. Lettieri, J. H. Haeni, and D. G. Schlom (unpublished).

[84]V. V. Il'chenko, G. V. Kuznetsov, V. I. Strikha, and A. I. Tsyganova, Mikroelektronika **27**, 340 (1998) [Russ. Microelectron **27**, 291 (1998)].

[85]V. V. Il'chenko and G. V. Kuznetsov, Pis'ma Zh. Tekh. Fiz. **27**, 58 (2001) [Tech. Phys. Lett. **27**, 333 (2001)].

[86]The destructive reaction at the alkaline earth oxide/Si interface has been observed over a range of temperatures from 580 to 630 °C depending on the quality of the interface and wafer vicinality. Never has the interface been seen to withstand temperatures above 700 °C.

[87]G. A. Costa, M. Ferretti, E. A. Franceschi, and G. L. Olcese, Thermochim. Acta **133**, 17 (1988).

[88]S. G. Tresvyatskii, L. M. Lopato, A. E. Kushchevskii, and A. V. Shevchenko, Inorg. Mater. (Transl. of Neorg. Mater.) **7**, 1681 (1971).

[89]S. G. Tresvyatskii, V. N. Pavlikov, L. M. Lopato, and L. I. Lugin, Inorg. Mater. (Transl. of Neorg. Mater.) **6**, 33 (1970).

[90]L. M. Lopato, L. I. Lugin, and A. V. Shevchenko, Sov. Progr. Chem. **39**, 27 (1973).

[91]L. M. Lopato, I. M. Maister, and A. V. Shevchenko, Inorg. Chem. **8**, 749 (1972).